Int. J. Electrochem. Sci., 15 **(2020)** 10664 – 10673, doi: 10.20964/2020.11.47

International Journal of
ELECTROCHEMICAL
SCIENCE
www.electrochemsci.org

Electrochemical Evaluation of Niobium Corrosion Resistance in Simulated Anodic PEM Electrolyzer Environment

Andrea Kellenberger[1,*], *Delia Duca*[1], *Nicolae Vaszilcsin*[1], *Corneliu Marius Craciunescu*[2]

[1] Politehnica University Timisoara, Faculty of Industrial Chemistry and Environmental Engineering,
[2] Politehnica University Timisoara, Faculty of Mechanical Engineering,
Piata Victoriei No. 2, RO-300006, Timisoara, Romania
[*]E-mail: andrea.kellenberger@upt.ro

Received: 15 July 2020 / *Accepted:* 4 September 2020 / *Published:* 30 September 2020

As cost reduction of stack components in proton exchange membrane (PEM) electrolyzers is needed, less expensive materials coated with anti-corrosive layers replace the state-of-the-art bipolar plates manufactured from massive titanium. One of the metals used for this purpose is niobium. In this work, we investigate the corrosion resistance properties of pure metallic niobium in simulated PEM electrolyzer environment. A corrosion test protocol was developed, including electrochemical impedance spectroscopy measurements, potentiodynamic polarization up to an anodic potential of 2 V followed by an accelerated stress test at 2 V for 6 hours. All tests were performed in O_2 saturated acid solutions, at 90°C to simulate the conditions at the anode side of PEM electrolyzers. In addition, interfacial contact resistance (ICR) measurements and scanning electron microscopy (SEM) imaging were performed both before and after the accelerated stress test. The presence of O_2 extends the potential range of the passive region as compared to solution without O_2 and the temperature increase leads to lower passivation and corrosion current densities. The passive oxide layer formed at higher temperatures is thicker, more compact and shows higher polarization resistance.

Keywords: Niobium, corrosion resistance, bipolar plates, PEM electrolysis

1. INTRODUCTION

Environmental issues represent nowadays an increasing global concern. One of the major causes of air pollution and global warming, with negative consequences for humans and the environment, is the dependence on fossil fuels. Efforts are made to replace fossil fuels with hydrogen obtained by electrolysis, especially in view of grid balancing caused by the fluctuations of renewable energy sources [1, 2]. The most suitable technology for coupling with renewables is proton exchange membrane electrolysis, since it complies with most of the grid constrains [3, 4, 5]. Even if PEM electrolyzers are one of the most viable option for sustainable hydrogen production, they still have to overcome some

challenges, like durability issues and high production costs [6, 7]. Recent trends in research aim to decrease the operation costs (OPEX) by increasing efficiency and reducing electricity costs, or decrease the capital expenditure (CAPEX) by reducing the production costs, increasing operating current density and decreasing the price of materials used for manufacture [8, 9]. Currently there are two main classes of materials used for the fabrication of bipolar plates (BPPs), the key component of a PEM electrolyzer: carbon or graphite base composites and metallic materials. Conventional graphite BPPs have high corrosion resistance and low interfacial contact resistance but high gas permeability, low flexure strength and toughness, and requires expensive technology for manufacturing the flow fields. On the other side, metallic BPPs can be easily deformed, have superior manufacturability and better electrical conductivity, are non-porous materials and some are corrosion resistant due to the formation of a thin passive oxide layer [10]. The corrosion resistance of BPP is one of the main requirements in PEM electrolyzers, due to the acid environment, which causes significant corrosion problems, thus an important increase of the materials and production costs of different components. This is especially relevant at the anode side of PEM electrolyzers, due to the harsh environmental conditions, in particular the high potential and the presence of pure oxygen. To overcome corrosion related problems, BPPs are currently manufactured from massive titanium [6, 11], sometimes with an additional platinum coating [12] to reduce the anodization process and lower the contact resistance. Less expensive base metals, such as stainless steel, aluminum or copper, protected by anticorrosive layers, represent a viable alternative to titanium. As corrosion-resistant coatings for stainless steel, Au and TiN have been tested [15], as well as titanium [13, 14] and niobium layers [9]. Niobium has the advantage of significantly lower prices compared to Au and Pt and shows excellent corrosion resistance properties conferred by a dense, protecting passive oxide layer, which forms spontaneously in air or aqueous solutions. Moreover, the corrosion resistance of un-coated metals such as molybdenum, tungsten, niobium, tantalum and various types of austenitic stainless steel has been evaluated at relevant PEM electrolyzer operating conditions [16] showing the necessity of protective, conductive coatings. An important factor, with critical influence on the degradation of the BPP material is the solution pH, which can increase the corrosion rate. The pH value inside an operating PEM water electrolysis cell was determined by recirculating feed water at the anode and cathode side and monitoring the pH value inside the two water tanks. It has been found that for operation at constant current density of 0.5 A cm^{-2} for 50 h at 50°C, the pH value drops to about 3.5 on the anode side and to 4.5 on the cathode side [15].

The aim of this work is to investigate the corrosion resistance properties of metallic niobium in conditions similar to those found inside an operating PEM electrolyzer, regarding anodic potential, temperature, pH and presence of oxygen. Since niobium based coatings deposited by different techniques start to be frequently used as anticorrosive protection layer for BPPs, it is important to have a reference regarding the electrochemical behavior of metallic niobium.

2. EXPERIMENTAL

Corrosion testing of metallic Nb was carried out using an Autolab PGSTAT 302N potentiostat/galvanostat and a water jacket three-electrode configuration corrosion cell. As working

electrode a 15 mm disc shaped metallic Nb (Sigma Aldrich, 99.8%) was used. As reference, a Ag/AgCl (3M KCl) electrode was positioned near the working electrode via a Luggin capillary and the counter electrode was a Pt gauze. Before measurement, the Nb electrode was mechanically polished with SiC paper of different grades up to 4000 and then mirror polished with diamond sprays with different grain sizes (6 and 3µm). Finally, it was cleaned by ultrasonication in ethanol. Corrosion test have been performed under conditions simulating the anode side environment of a PEM electrolyzer, in 0.05 M H_2SO_4 solution (pH = 1.4), at 90° C, in O_2 saturated solutions. A special protocol for the corrosion tests was developed [17], consisting in measurement of open circuit potential (OCP) followed by electrochemical impedance measurements (EIS) and potentiodynamic polarization curves recorded at scan rate of 1 mV s^{-1}. These three steps were repeated both before and after the metallic Nb sample is submitted to an accelerated stress test by polarization at 2V for 6 hours. For comparison, similar measurements were performed at ambient temperature.

EIS measurements were carried out using the FRA Module of Autolab 302N, at open circuit potential, in the frequency range from 100 kHz to 10 mHz and AC voltage amplitude of 10 mV rms. Each spectrum consist of 60 points, collected with a logarithmic distribution of 10 points / decade. A complex non-linear least squares Levenberg-Marquardt procedure was used to fit the experimental EIS data to the equivalent electrical circuit (EEC), using the ZView 3.0 software (Scribner Associates, Inc.).

The conductivity of metallic Nb sample before and after the accelerated stress test was evaluated by interfacial contact resistance measurements. For the ICR measurements, a sandwich-like assembly, consisting of the metallic Nb sample, placed between two pieces of untreated carbon paper (Spectracarb 2050A-6060), two gold-coated copper plates and two insulating plates was tested under compression in a tensile testing machine HDZ in the range 0-2kN. This set-up is similar to that reported elsewhere [17]. A direct current of 1A was applied between the two gold plated copper plates using a power source and the voltage was measured with a precision multimeter Picotest M3510A. The applied compaction force was increased in steps, from 50 to 1400 N, which corresponds to a compaction pressure of approximately 30 to 800 N cm^{-2}. An electrical equivalent circuit modeled the sandwich-like assembly, consisting of several resistors connected in series, where each resistor corresponds to a contact resistance and the ICR of Nb was calculated.

The structure and morphology of the passive oxide layer on the surface of metallic Nb and its composition were investigated using a TESCAN Vega 3 LM scanning electron microscope, equipped with a Bruker Quantax 200 Energy Dispersive X-ray Spectroscopy (EDX) system with Peltier-cooled XFlash 410M silicon drift detector. The surface porosity was estimated by image analysis, using ImageJ, a public domain software [18].

3. RESULTS AND DISCUSSION

Potentiodynamic polarization curves obtained on metallic Nb at ambient temperature in solutions with and without oxygen, as well as at 90° C in oxygen saturated acid solution are shown in

Figure 1. The potentiodynamic characteristics of metallic Nb after the accelerated stress test at both ambient and 90° C are also presented in Figure 1.

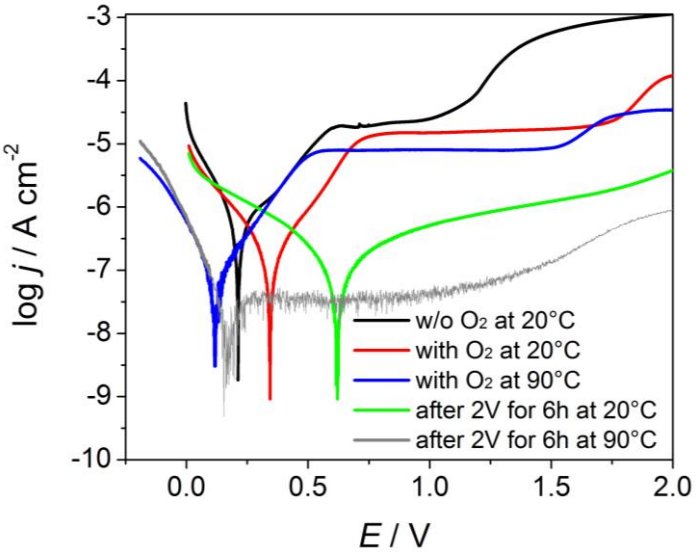

Figure 1. Potentiodynamic polarization curves (scan rate 1 mV s^{-1}) on metallic Nb in the absence of oxygen at 20° C and in oxygen saturated 0.05 M H_2SO_4 solution (pH = 1.4), before and after the accelerated stress test, at temperatures of 20 and 90° C.

Before the accelerated stress test, the shape of the polarization curves is typical for anodic passivation of niobium, showing three distinct regions on the anodic branch. The first region corresponds to the active region, where metal dissolution takes place and the current increases exponentially with the applied potential. The second or passive region corresponds to the formation of passive oxide layer and the anodic current is independent on the applied potential. Finally, the third region is the transpassive region, where dissolution of passive films takes place, sometimes masked by oxygen evolution reaction. It can be observed that the active/passive transition is influenced by both temperature and presence of oxygen. It takes place at more negative potentials in the absence of oxygen and at more positive potentials in O_2 saturated solutions. The temperature increase up to 90° C shifts the passivation potential to more negative values. It is worth noticing that the potential range corresponding to the passive region is extended from about 400 mV in the absence of oxygen to about 1000 mV in the presence of oxygen, at both temperatures. Near the corrosion potential, both cathodic and anodic processes are under activation control, followed by a passive anodic behavior at more positive potentials. In the absence of oxygen, the cathodic process is the hydrogen evolution reaction and the cathodic branch shows a Tafel behavior, with a slope closed to the theoretical value. In the presence of oxygen, the cathodic slope increases, showing that the cathodic process also implies oxygen reduction reaction. This effect is more pronounced at lower temperature, since the solubility of oxygen decreases with temperature.

After the accelerated stress test, the polarization curves at both 20 and 90° C display a passive anodic behavior and the current has a very low and constant value, indicating the formation of a stable, corrosion-resistant passive oxide layer. Also, the corrosion potential shifts to more positive values, by 280 mV when the stress test is carried out at 20° C and by 70 mV at 90° C.

The corrosion parameters, i.e. corrosion potential (E_{corr}), corrosion current (i_{corr}) and corrosion rate (v_{corr}) have been determined from the Tafel plots given in

Figure 1b. The Stern-Geary equation (1) was used to calculate polarization resistances (R_p).

$$R_p = \frac{b_a \cdot b_c}{j_{corr} \cdot 2.303(b_a + b_c)} \quad (1)$$

where: R_p is the polarization resistance, Ω cm^2; b_a and b_c are the anodic and cathodic Tafel slopes, V and j_{corr} is the corrosion current density, A cm^{-2}.

Table 1 summarizes the values of corrosion parameters obtained from the Tafel plots.

Table 1. Corrosion parameters of metallic Nb in 0.05 M H_2SO_4 solution (pH = 1.4) at 20 and 90° C, before and after the accelerated stress test.

Corrosion parameters	**w/o O_2 @ 20° C**	**O_2 saturated @ 20° C**		**O_2 saturated @ 90° C**	
	before	before	after	before	after
E_{corr} / V	0.213	0.343	0.622	0.121	0.193
j_{corr} / µA cm^{-2}	0.45	0.17	0.16	0.08	0.02
j_{pass} / µA cm^{-2}	19	15	0.5	8	0.05
b_a / mV decade^{-1}	237	184	705	153	570
b_c / mV decade^{-1}	-143	-222	-453	-182	-118
v_{corr} / µm y^{-1}	3.2	1.2	1.2	0.6	0.2
R_p / kΩ cm^2	85.3	261.6	739.2	443.4	2011.8

In O_2 saturated solutions, the corrosion potential E_{corr} shifts to more positive values and the corrosion current density and corrosion rate also decrease. An important increase of the polarization resistance is also observed, indicating that the formation of the passive oxide film is favored by the presence of oxygen. Comparing corrosion parameters before and after the accelerated stress test, it can be concluded that a stable passive oxide film is formed, as indicated by the decrease of corrosion current and corrosion rate and the increase of both anodic slope and polarization resistance.

The chronoamperometric curves measured during the accelerated stress test conducted at 2 V for 6 h, are given in Figure 2. Both curves show an exponential decay of the current density in time, corresponding to the growth of the protective oxide layer. The current density values stabilize around 3 µA cm^{-2} at 20° C and 1 µA cm^{-2} at 90° C, indicating the formation of a stable anodic oxide film.

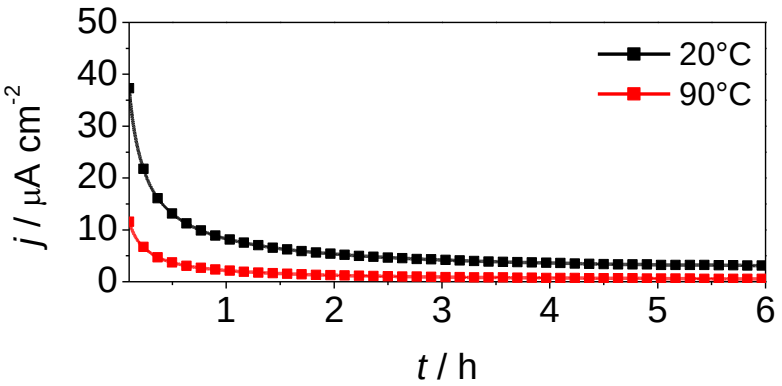

Figure 2. Chronoamperometric curves of metallic Nb in O_2 saturated 0.05 M H_2SO_4 solution (pH = 1.4) at 20 and 90° C, during the accelerated stress test at E = 2 V for 6 h.

Electrochemical impedance measurements were conducted at the open circuit value, before and after the accelerated stress test at 20 and 90° C and the corresponding Nyquist and Bode plots are displayed in Figure 3.

All Nyquist plots in Figure 3a show a single capacitive loop with a lower diameter at 20°C and a higher diameter at 90° C. After the stress test, the diameter of the capacitive loop, which is related to the polarization resistance is increased, as a result of the formation of the passive oxide layer on the surface. At high frequencies the Bode plots in Figure 3b display a frequency independent behavior of the absolute impedance and phase angle values closed to 0°, corresponding to the resistive response of the solution, R_S. In the mid-to-low frequency region, the absolute impedance increases with a constant slope of almost 1 and the maximum phase angle value is closed to -80°C, which indicates a capacitive response of the oxide film. The impedance data were modeled to a simple electric equivalent circuit (EEC), consisting of the solution resistance R_S in series with a parallel connection of the oxide capacitance and the polarization resistance R_p.

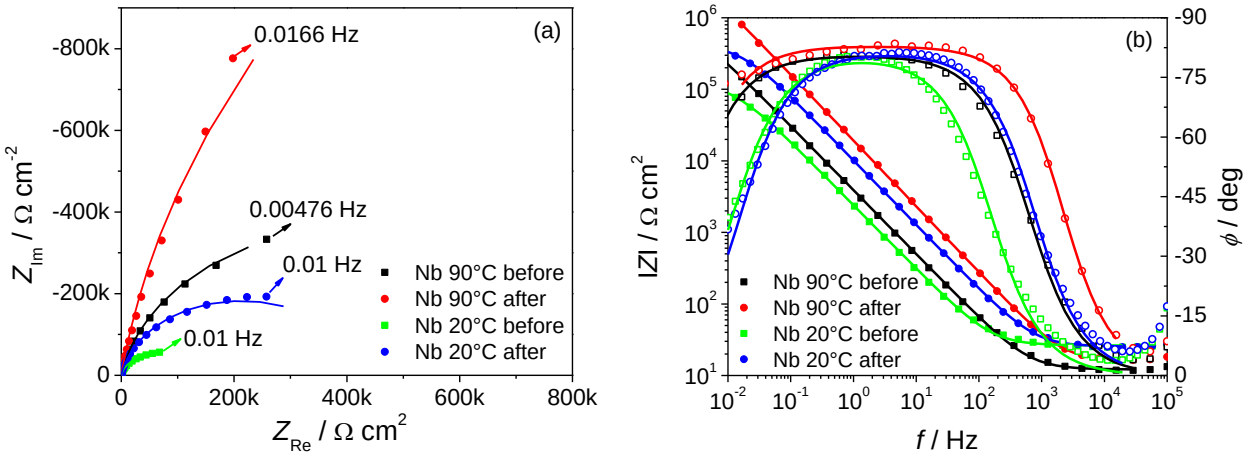

Figure 3. Nyquist (a) and Bode (b) plots of metallic Nb in O_2 saturated 0.05 M H_2SO_4 solution (pH = 1.4) measured at open circuit potential, at 20 and 90° C. Symbols are experimental data and continuous lines are simulated by fitting.

Table 2. Results of EIS fitting of metallic Nb in 0.05 M H_2SO_4 solution (pH = 1.4) at different temperatures, before and after polarization at 2 V for 6 h, at open circuit potential.

Parameter	**O_2 saturated @ 20° C**		**O_2 saturated @ 90° C**	
	before	after	before	after
R_S / Ω	26.2 (1.0%)	25.3 (0.8%)	12.2 (0.9%)	16.1 (0.7%)
CPE-T / F cm^{-2} s^{n-1}	8.07×10^{-5} (0.9%)	1.87×10^{-5} (0.6%)	4.94×10^{-5} (0.5%)	9.59×10^{-6} (0.4%)
n	0.89 (0.3%)	0.90 (0.1%)	0.90 (0.1%)	0.92 (0.1%)
R_p / kΩ cm^2	126.3 (3.0%)	425.3 (1.7%)	860.6 (3.7%)	5572.5 (6.0%)
C_{ox} / F cm^{-2}	3.77×10^{-5}	7.97×10^{-6}	2.17×10^{-5}	4.47×10^{-6}
d_{ox} / nm	1.0	4.6	1.7	8.1
χ^2	7.2×10^{-3}	2.9×10^{-3}	3.0×10^{-3}	1.5×10^{-3}

To account for the surface inhomogeneity the ideal capacitance was replaced by a constant phase element (CPE). In contrast to an ideal capacitance, which shows a phase angle of -90°, the constant phase element has a phase angle of –(*n**90°), where *n* is a parameter between 0 and 1. The results of fitting EIS data to the EEC are given in Table 2 together with the standard errors and the quality of fit expressed by the χ^2 value.

If the passive oxide layer is regarded as a dielectric material between the electrolyte and the Nb surface, its capacitance can be expressed according to relation (2):

$$C_{ox} = \frac{\varepsilon \varepsilon_0 A}{d_{ox}} \quad (2)$$

where ε is the relative dielectric constant, ε_o is the permittivity of vacuum (8.85×10^{-14} F cm^{-1}), A is the effective surface area and d_{ox} is the thickness of the oxide layer. For anodically formed amorphous oxide films on niobium, a dielectric constant value of 41 was reported [19]. This relationship allows calculating the values of the oxide layer thickness, which are also given in Table 2. It can be observed that the passive oxide layer is present on the Nb surface even before polarization at 2 V because it forms spontaneously in air and its thickness increases during stabilization of OCP values in O_2 saturated solutions. After passivation an almost five times thickening of the oxide layer is observed at both 20 and 90° C. Oxide layer thicknesses are in agreement with literature data, which indicate an oxide formation factor of 2.7 nm V^{-1} for the anodization of Nb in 0.1 M sulfuric acid at room temperature [20]. Polarization resistance values determined by EIS are in the same range with those calculated with the Stern-Geary equation.

The structure of the passive oxide layer formed in O_2 saturated solution at different temperatures was investigated by SEM and the composition was determined by EDX.

Figure 4 shows the SEM images of the anodic oxide layer obtained after polarization at 2 V for 6 h, in O_2 saturated solutions at 20 and 90° C.

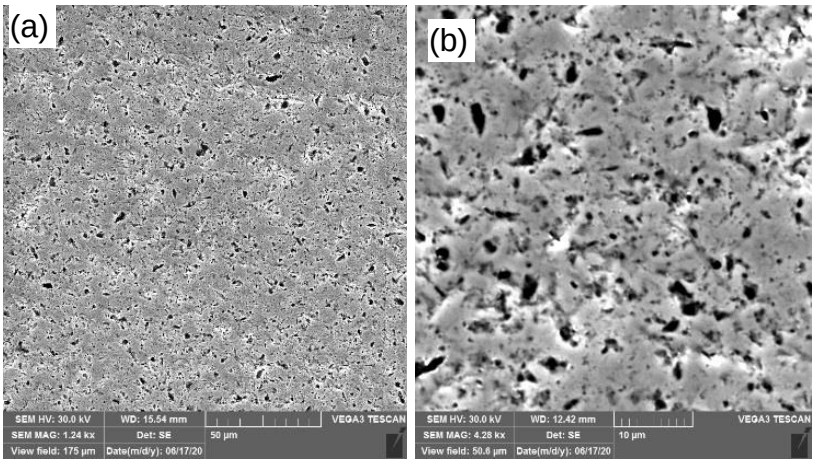

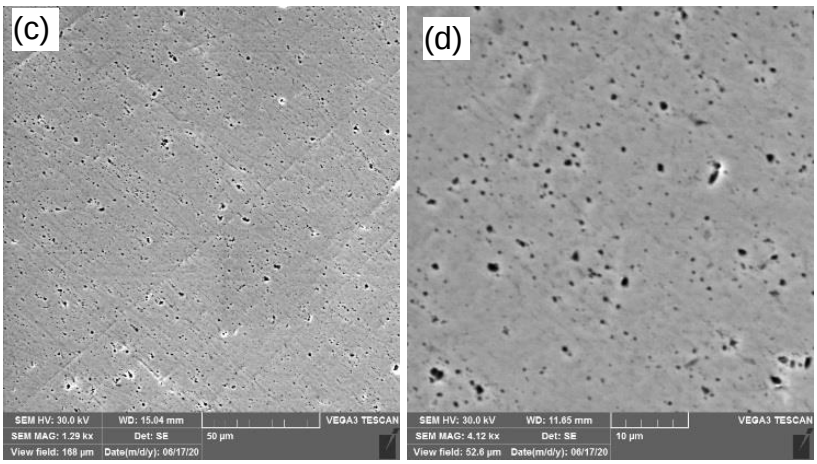

Figure 4. SEM images at different magnifications of the passive oxide layer formed on metallic Nb after passivation at 2 V for 6 h, in O_2 saturated 0.05 M H_2SO_4 solution at (a,b) 20° C and (c,d) 90° C.

The passive layer formed at 20° C shows a rough and porous structure, in contrast to the layer obtained at 90° C, which shows a smoother and more compact structure. The porosity determined by image analysis is 22.1 % and 2.9 % for the oxide layers formed at 20° C and respectively 90° C. These results are in agreement with the electrochemical measurements, which also show that a more protective oxide layer forms at higher temperature, with almost three times higher polarization resistance than at lower temperature. EDX analysis gave about 52 at % Nb and 48 at % O, however these values does not reflect the exact stoichiometric composition of the oxide. This can be explained since the X-ray penetration depth is in the range of about 0.5-3 µm, depending on the energy of the incident beam and the density of the material, but the oxide layer thickness is in the range of several nanometers [21, 22]. In addition, the oxide layer is usually composed of various oxide forms with different stoichiometry [22].

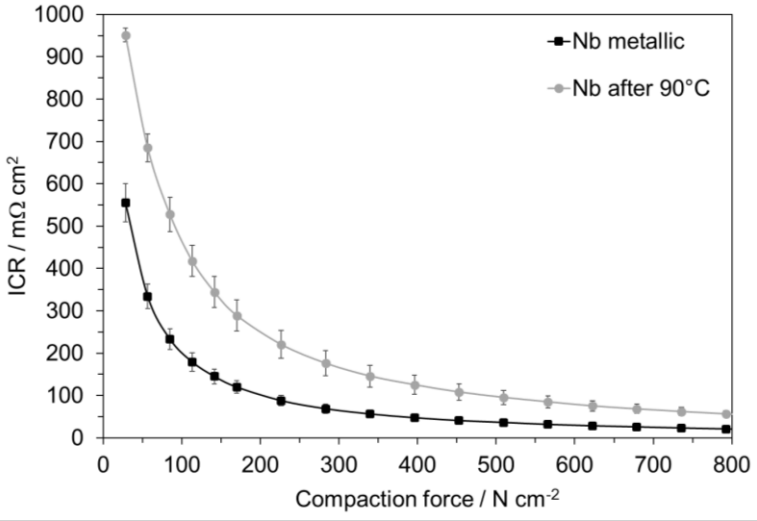

Figure 5. Results of ICR versus compaction force measurements of metallic Nb and Nb after passivation at 2 V for 6 h, in O_2 saturated 0.05 M H_2SO_4 solution (pH = 1.4) at 90° C.

The interfacial contact resistance of Nb was measured before and after passivation at 2 V for 6 h, at 90° C. The results of ICR measurements versus the applied compaction force are displayed in Figure 5. ICR values of metallic Nb and Nb polarized at 2 V for 6 h, decrease significantly when the compaction force increases, especially at low compaction forces, due to the improved electrical contact inside the sandwich-like assembly used for the measurement. As expected, the ICR of polarized Nb is higher than that of metallic Nb, due to the formation of the passive oxide layer. At the highest compaction force, the ICR of polarized Nb is 55 mΩ cm^2 as compared to 20 mΩ cm^2 for metallic Nb. Literature data [9] indicate that the pressure usually applied for assembling commercial PEM electrolyzer stacks is in the range of 120 to 200 N cm^{-2}. Within this range the ICR of polarized Nb decreases from 400 to 250 mΩ cm^2 and are 2.5 times higher than for metallic Nb. ICR values of Nb polarized at 2 V have been reported to be about 150 mΩ cm^2 at 140 N cm^{-2} [16] as compared to 345 mΩ cm^2 obtained in this study. Different conditions used during polarization may explain the dissimilar values. In our study, the polarization was performed at 90° C, for 6 h, in O_2 saturated solution, at pH 1.4, as compared to 70° C, for 1 h, in the absence of O_2 and at pH 5.5 [16]. The differences in temperature, polarization time, solution pH and O_2 saturation lead to a different thickness of the passive oxide layer, probably also a different structure and morphology, which can explain the higher ICR value obtained in our study.

4. CONCLUSIONS

Corrosion resistance properties of metallic Nb in simulated PEM electrolyzer environment were studied by electrochemical impedance spectroscopy and potentiodynamic polarization up to 2 V. Corrosion parameters were determined before and after an accelerated stress test at 2 V for 6 hours, in O_2 saturated acid solution of pH = 1.4, both at 20 and 90° C. The effect of oxygen presence and temperature increase on the electrochemical behavior of Nb was established. It has been found that the presence of oxygen shifts the transpassivation potential to more positive values, thus increasing the potential window of the passive region. In addition, lower passivation and corrosion current densities, as well as higher polarization resistances were obtained in the presence of oxygen. After polarization at 2 V for 6 hours the thickness of the passive layer determined from EIS measurements increases from 1.7 to 8 nm at 90° C and the corrosion rate decreases to 0.2 μm y^{-1}. SEM imaging shows a compact structure of the Nb oxide film formed at 90° C and a change of the porosity from 22 to 3% as the temperature increases from 20 to 90° C. ICR values obtained after the accelerated stress test at 90° C are 2.5 times higher than for metallic Nb. In conclusion, the presence of oxygen, high temperatures and high potentials in acidic media, which are conditions similar to those found in operating PEM electrolyzers doesn't have a negative impact on the corrosion resistance of metallic Nb, due to the formation of a very stable, low porosity, protective oxide layer.

ACKNOWLEDGMENTS

This project has received funding from the Fuel Cells and Hydrogen 2 Joint Undertaking under grant agreement No 779478. This Joint Undertaking receives support from the European Union's Horizon 2020 research and innovation programme, Hydrogen Europe and Hydrogen Europe research.

References

1. A. Buttler and H. Spliethoff, *Renew. Sust. Energ. Rev.*, 82 (2018) 2440. https://doi.org/10.1016/j.rser.2017.09.003
2. D.S. Falcão and A.M.F.R. Pinto, *J. Clean. Prod.*, 261 (2020) 121184. https://doi.org/10.1016/j.jclepro.2020.121184
3. L. Allidières, A. Brisse, P. Millet, S. Valentin and M. Zeller, *Int. J. Hydrogen. Energy*, 44 (2019) 9690
4. A. Hernandez-Gomez, V. Ramirez and D. Guilbert, *Int. J. Hydrogen. Energy*, 45 (2020) 14625. https://doi.org/10.1016/j.ijhydene.2020.03.195
5. C.-H. Je, H.-M. Kim, *Int. J. Electrochem. Sci.*, 14 (2019) 6948. https://doi.org/10.20964/2019.07.64
6. S. Shiva Kumar and V. Himabindu, *Mater. Sci. Energ. Technol.*, 2 (2019) 442. https://doi.org/10.1016/j.mset.2019.03.002
7. M. Schalenbach, A. R. Zeradjanin, O. Kasian, S. Cherevko and K. J. J. Mayrhofer, *Int. J. Electrochem. Sci.*, 13 (2018) 1173. https://doi.org/10.20964/2018.02.26
8. S.A. Grigoriev, V.N. Fateev, D.G. Bessarabov and P. Millet, *Int. J. Hydrogen. Energy*, *in press*, 2020. https://doi.org/10.1016/j.ijhydene.2020.03.109
9. P. Lettenmeier, R. Wang, R. Abouatallah, B. Saruhan, O. Freitag, P. Gazdzicki, T. Morawietz, R. Hiesgen, A.S. Gago and K.A. Friedrich, *Sci. Rep.*, 7 (2017) 44035. doi: 10.1038/srep44035 (2017)
10. V. Mehta and J.S. Cooper, *J. Power. Sources*, 114 (2003) 32. doi: 10.1016/S0378-7753(02)00542-6
11. M. Carmo, D. L. Fritz, J. Mergel and D. Stolten, *Int. J. Hydrogen. Energy*, 38 (2013) 4901. https://doi.org/10.1016/j.ijhydene.2013.01.151
12. O. K. Alekseeva, E. K. Lutikova, V. V. Markelov, V. I. Porembsky and V. N. Fateev, *Int. J. Electrochem. Sci.*, 13 (2018) 797. https://doi.org/10.20964/2018.01.79
13. A.S. Gago, S.A. Ansar, B. Saruhan, U. Schultz, P. Lettenmeier, N.A. Cañas, P. Gazdzicki, T. Morawietz, R. Hiesgen, J. Arnold and K.A. Friedrich, *J. Power. Sources*, 307 (2016) 815. https://doi.org/10.1016/j.jpowsour.2015.12.071
14. P. Lettenmeier, R. Wang, R. Abouatallah, F. Burggraf, A.S. Gago and K.A. Friedrich, *J. Electrochem. Soc.*, 163 (2016) F3119. https://doi.org/10.1149/2.0141611jes
15. M. Langemann, D.L. Fritz, M. Müller and D. Stolten, *Int. J. Hydrogen. Energy*, 40 (2015) 11385. https://doi.org/10.1016/j.ijhydene.2015.04.155
16. S. Lædre, O.E. Kongstein, A. Oedegaard, H. Karoliussen and F. Seland, *Int. J. Hydrogen. Energy*, 42 (2017) 2713. https://doi.org/10.1016/j.ijhydene.2016.11.106
17. A. Kellenberger, N. Vaszilcsin, D. Duca, M.L. Dan, N. Duteanu, S. Stiber, T. Morawietz, I. Biswas, S.A. Ansar, P. Gazdzicki, F.J. Wirkert, U. Rost, A.S. Gago and K.A. Friedrich, *Manuscript in preparation* (2020).
18. W.S. Rasband (1997–2005) ImageJ, U. S. National Institutes of Health, Bethesda, Maryland, USA, http://rsb.info.nih.gov/ij/
19. L. Young, *Can. J. Chem.*, 38 (1960) 1141.
20. J.P. Kollender, C.C. Mardare, I.A. Mardare, A.W. Hassel, *J. Sol. State. Electrochem.*, 22 (2018) 2457. https://doi.org/10.1007/s10008-018-3957-4
21. I.L. Arsova, A.R. Prusi and L.D. Arsov, *J. Solid. State. Electrochem.*, 7 (2003) 217. https://doi.org/10.1007/s10008-002-0303-6
22. I. Arsova, A. Prusi, T. Grčev and L. Arsov, *J. Serb. Chem. Soc.*, 71 (2006) 177. https://doi.org/10.2298/JSC0602177A